Research article

Experimental evaluation of cement integrity on exposure to supercritical CO_2 using NMR: Application to geostorage

Sidi Mamoudou [*], Mark Curtis, Son Dang, Chandra Rai

Mewbourne School of Petroleum and Geological Engineering, University of Oklahoma, United States

ARTICLE INFO

ABSTRACT

Carbon sequestration is one approach to achieve carbon dioxide reduction in the atmosphere. Underground storage of CO_2 requires an understanding of geochemical and geomechanical alteration on the integrity of the injection wellbore. In this study, we investigate the reactivity of supercritical CO_2 (scCO_2) at 65 °C and 20.7 MPa on Portland class G cement plugs used for oil and gas well completion, for exposure of up to 5 weeks.

For nanoporous media, such as cement, diffusion is believed to be the major mass transport mechanism (Perkins and Johnston, 1963) [1]. To quantify the extent of the alteration (mineralization/dissolution) on fluid diffusivity through the cement matrix, a novel approach based on Nuclear Magnetic Resonance (NMR) is employed to derive diffusional tortuosity. Comparing pre- and post-scCO_2 exposure, deuterium oxide (D_2O) intrusion profiles allow us to determine flow path alteration in the cement plugs. Additional characterizations include Fourier Transform Infrared Spectroscopy (FTIR) to observe the change in cement composition, micro X-ray Computed Tomography (μXCT), along with Scanning Electron Microscopy (SEM) and Energy Dispersive Spectroscopy (EDS) to determine invasion extent and microstructure modifications, Mercury Injection Capillary Pressure (MICP) for pore throat size distribution and BET N_2 isothermal adsorption for surface area and pore size distribution.

The results show that exposure to scCO_2 promotes both calcium carbonate precipitation and dissolution simultaneously. However, the alteration is pore size dependent. After 5 weeks of exposure, there is evidence of carbonate dissolution in smaller pores (<30 nm) and both precipitation and dissolution in larger pores (30–200 nm). The alteration of the cement plugs leads to a decrease in the storage and connectivity of the cement. The porosity decreased from 37 to 33 % in 5 weeks, while the matrix tortuosity increased by 6 and 3 times after 2 and 5 weeks of exposure, respectively. The experimental results imply that the cement carbonate precipitation can limit the migration of scCO_2 through the cement matrix.

This work also highlights an alternative laboratory approach to quantify the risk associated with scCO_2 exposure on Portland cement using NMR-derived tortuosity.
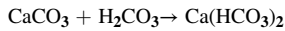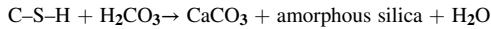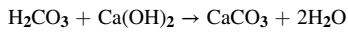
1. Introduction

Carbon capture and storage (CCS) in the subsurface offers a viable option for reducing atmospheric CO_2 levels. However, for long-term geologic storage of CO_2, it is crucial to assess the risk of leakage along the wellbore components. In oil and gas wells, class G or H

---

* Corresponding author.
  E-mail address: sidi.mamoudou@ou.edu (S. Mamoudou).

Portland cement is commonly utilized to seal the wellbore annulus and the reservoir formation. Under storage conditions, CO_2 in a supercritical state can react with cement components, namely calcium hydroxide ($Ca(OH)_2$) and calcium silicate hydrates (C–S–H), resulting in the formation of calcium carbonate ($CaCO_3$) [2–11].

The carbonation reaction can be divided into three phases: (i) CO_2 dissolution in the brine, forming carbonic acid (H_2CO_3), (ii) degradation of $Ca(OH)_2$ and/or calcium silicate hydrates, leading to the formation of calcium carbonates and amorphous silica, and (iii) conversion of calcium carbonate into calcium bicarbonate [12].

$$H_2CO_3 + Ca(OH)_2 \rightarrow CaCO_3 + 2H_2O$$

$$C–S–H + H_2CO_3 \rightarrow CaCO_3 + amorphous\ silica + H_2O$$

$$CaCO_3 + H_2CO_3 \rightarrow Ca(HCO_3)_2$$

Several studies have investigated the degradation of Portland cement by CO_2 using either batch exposure or flow-through experiments. Barlet-Gouédart et al. [13] and Rimmelé et al. [14] conducted static batch measurements at 90 °C and 27 MPa on cement exposed to $scCO_2$ and saturated CO_2 brine. They observed that carbonation follows a sealing stage related to calcium carbonate precipitation, plugging the pores, followed by a dissolution stage marked by a significant increase in porosity. Kutchko et al. [2,3] focused on the cement's microstructure during carbonation, revealing three distinctive zones: the unaltered cement, a zone depleted in portlandite, a calcium carbonated zone, and a residual amorphous silica zone. They also observed limited invasion of the carbonated front, estimated to progress around a few millimeters after 20–30 years.

Later, flow-through experiments were carried out to observe the dynamic impact of carbonation. Wigan et al. [15] focused on fractured cement (cement-caprock interface) at 54 °C and 19.9 MPa under $scCO_2$ injection, observing an increase in fracture aperture. Huerta et al. [16] observed the self-healing of fractures with the injection of brine-saturated CO_2 at room temperature, postulating that fracture aperture and CO_2 residence time control mineralization inside the fracture. However, Luquot et al. [17] reported that the fracture aperture after carbonation was related to the injection flow rate. Mason et al. [18] investigated mechanical property changes near the carbonated zone, finding that Young's modulus in the depleted, carbonate, and amorphous layers decreased to approximately 75 %, 64 %, and 34 % respectively of the unaltered cement after 8 days of exposure. Finally, Walsh [19,20] investigated the impact of fracture geometry between the cement and the caprock, finding that changes in permeability depended on the initial fracture geometry.

Most of the highlighted studies, whether batch or flooding, have focused on measuring transport alterations (porosity and permeability) on dried samples. However, drying cement induced damage such as microcracking, fine pore collapse, and mineralogical transformation [21].

To evaluate the flow quality of porous media, permeability is usually considered as the controlling transport parameter. Perkins and Johnston [1] defined the general convective coefficient in porous media including both the advective term (governed by permeability, pore throat size, and displacing velocity), and the diffusion term (governed by bulk fluid diffusivity and matrix tortuosity).

$$K_l = \frac{D_o}{F\varnothing} + 0.5Ud_p\sigma \qquad\qquad 1$$

in which K_l is the overall dispersion coefficient, the first term is associated with the dispersion by diffusion: D_o is the mutual fluid diffusivity, $F\varnothing$ represents tortuosity, the second term is associated with the dispersion by advection/mechanical mixing: U is viscous flow velocity (controlled by permeability), d_p is characteristic pore throat diameter, and σ is porous heterogeneity. Previous studies have shown that in nanoscale porous media such as cement, the contribution of advection is relatively small, which makes diffusion the dominant drive mechanism [1,22].

Water is an essential component of the cement hydration reaction and its microstructure. Therefore, removing it to characterize various properties (such as cement porosity and pore size distribution) is not recommended [23]. Drying the cement sample before measuring gas permeability, as noted by Gallé [21] and Collier et al. [24], may damage the pore structure.

As demonstrated previously by Blinc et al. [25] and Ichim et al. [23], NMR can accurately assess cement water volume while keeping the sample hydrated.

In our study, we measure tortuosity, rather than permeability, by observing the effective diffusion of a doping agent using NMR on both pre-and post-exposed cement to CO_2. This method allows evaluation while keeping the cement wet throughout the entire experiment and thus removing potential drying artifacts.

2. Theory and/or methods

2.1. Sample description and exposure

Class G cement typically used for oil/gas well completion was used in this study. A total of 3 cement samples (1x1in) were used; one intact and 2 exposed to $scCO_2$ for 2 and 5 weeks, respectively. The plugs were used for D_2O diffusivity, while companion disks (0.25x1in) were used to measure SEM, µXCT, MICP, and BET. The cement plugs were cured at 65 °C for 30 days. These plugs had a total porosity of 37 $\pm$ 2 %. The X-ray fluorescence mineralogy of the untreated sample is given in Table 1.

Fig. 1 shows the experimental workflow used in this study. The samples were vacuum imbibed in a brine solution (1.2 % KCl, 1.2 % NaCl, and 3.6 % $CaCl_2$) to match the salinity and resistivity of the solution used to cure the cement samples and ensure 100 %

saturation. A D_2O-brine solution with a similar salt concentration was prepared to monitor the diffusivity of D_2O into the cement matrix pre- and post-exposure.

After imbibition for 48 h, all samples except the control samples were exposed to $scCO_2$ at 65 °C and 20.7 MPa for 2 and 5 weeks inside a Parr reactor, as shown in Fig. 2, and intrusion of D_2O into the cement plug was monitored as a function of time using NMR. This data allowed us to calculate the diffusivity of D_2O in the cement plugs.

2.2. Diffusional tortuosity

A 12 MHz Oxford Geospec™ spectrometer (TE = 114 μsec) with a Green Imaging acquisition and processing software was used to acquire the total T_2 signal, which is calibrated to determine H_2O intensity within the cement matrix. The T_2 relaxation represents the relaxation or decay of hydrogen protons in the pore fluid after exposure to a magnetic field. The area under a T_2 distribution is directly proportional to the amount of hydrogen-based fluid present in the sample. NMR T_2 is governed by equation (2):

$$\frac{1}{T_2} = \frac{1}{T_{2\,bulk}} + \rho_2 \frac{S}{V} + D \frac{(\gamma\,G\,TE)^2}{12} \qquad\qquad 2$$

the subscript bulk indicates bulk relaxation time,

ρ_2 = the surface relaxivity
$\frac{S}{V}$ = Pore surface-to-volume ratio
D = bulk diffusion coefficient of the in-situ pore fluid
γ the gyromagnetic ratio
G is the magnetic field gradient
TE is the echo spacing time in a CPMG sequence.

For our experiment the 1st term and 3rd term can be dropped, thus the T_2 relaxation time is related to surface relaxivity and the pore surface-to-volume ratio. Eq. (2) can be simplified to:

$$\frac{1}{T_2} = \rho \frac{2}{r} \qquad\qquad 3$$

where r is the radius of the pore in nm, and ρ is the surface relativity of cement assuming carbonates, 5 μs/s [26–28]. Knowing the surface relaxivity of the minerals, T_2 distribution can also be converted to pore sizes [29].

Tortuosity measures the obstruction that fluid molecules must overcome to move through a porous medium. It is calculated as the ratio of the square root of the effective diffusivity of the fluid in the porous medium to the bulk fluid diffusivity (Eq. (4)). The effective diffusivity of the cement samples was calculated by measuring the reduction in NMR T_2 relaxation response during D_2O immersion pre- and post-exposure. The effective diffusivity of D_2O in the cement was derived by matching 1-D Fick's law of diffusion (Eq. (5)) assuming radial diffusion and the D_2O NMR intrusion profile. A detailed explanation is presented by Dang et al. [30] and Odiachi [31].

The following equation is used to estimate sample tortuosity from diffusivities:

$$\tau^{1/2} = \frac{D_{bulk}}{D_{eff}} \qquad\qquad 4$$

D_{eff} = Effective diffusivity of D_2O in cement
D_{bulk} = Bulk fluid diffusivity of H_2O in D_2O, 2.3×10^{-9} m^2/s at 25 °C [32]

$$\frac{\partial C_a}{\partial t} = D \frac{\partial^2 C_a}{\partial x^2} \qquad\qquad 5$$

C_a = Concentration of solute (kg/m^3)
D = Diffusion coefficient (m^2/s)
x = Time (s)
t = Distance from the interface (m)

2.3. Chemical and microstructural analysis

An FEI Helios Nanolab 600 Dualbeam FIB/SEM with a backscattered electron (BSE) detector and an Oxford X-MAX energy-dispersive spectrometer were used to determine microstructure and elemental changes on the surface of cement plugs pre- and post-exposure to $scCO_2$. The brightness of the BSE image reflects the average atomic number of a given phase composition. The depth of the altered zone was observed using μx-ray computed tomography in an Xradia XCT-400. Finally, transmission Fourier transforms

Table 1
X-ray fluorescence-derived mineralogy measured on the untreated cement, showing mostly CaO and SiO$_2$ components.

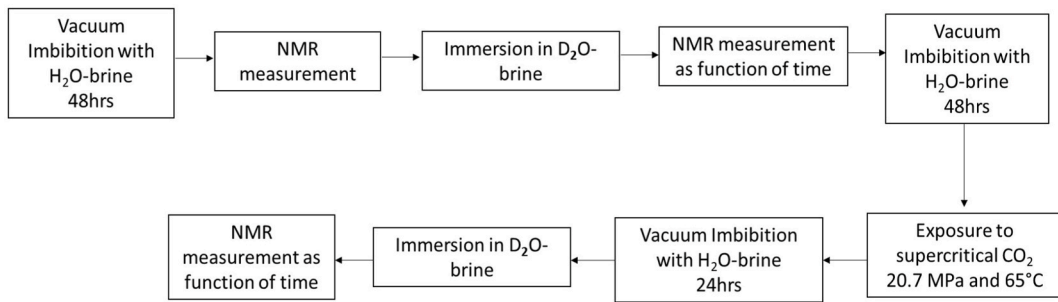|	MgO	CaO	K$_2$O	Fe$_2$O$_3$	SiO$_2$	Al$_2$O$_3$
composition (wt%)	2	64	1	8	19	6

Fig. 1. Experimental workflow used in the present study. Flow path alteration was determined by comparing D_2O diffusivity before and after exposure to $scCO_2$.
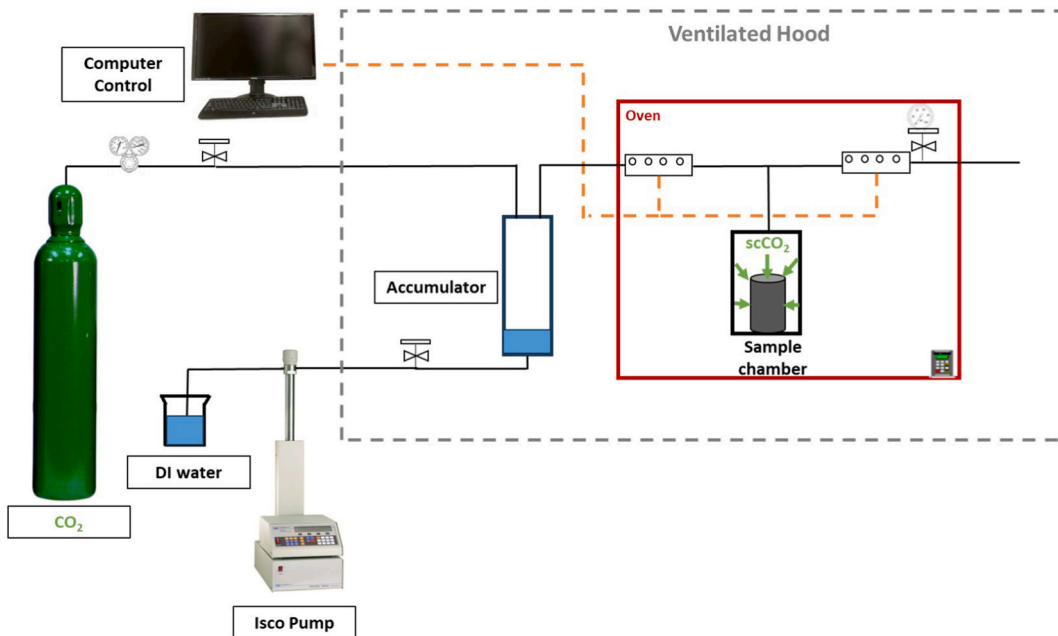

Fig. 2. Schematic of CO_2 exposure apparatus. Exposure was carried at 20.7 MPa and 65 °C, conditions at which CO_2 is in a supercritical state.

infrared spectroscopy was used to observe the change in different functional groups [33], reflecting the alteration in cement composition after gas exposure.

2.4. Pore structure alteration

Isothermal N_2 adsorption and mercury injection capillary pressure measurements on dried samples were used to characterize the change in surface area and pore throat size, respectively. BET surface area was conducted using a Micrometrics Tristar 2 apparatus. Density Functional Theory (DFT) assuming slit pore type was used to convert surface area to pore size [34]. For MICP, a Micrometrics AutoPores IV apparatus was used to capture pore throat size distribution, from 2 nm up to 20 μm with a maximum intrusion pressure of up to 415 MPa.

3. Results

3.1. Diffusional tortuosity

Fig. 3 shows the NMR T_2 relaxation of the control sample during immersion into D_2O-brine. Over time the NMR signal amplitude decreases as D_2O is gradually replacing the water inside the cement, from 6.7 to 2.3 ml. Fig. 4a and b show the impact of $scCO_2$ on the T_2 relaxation after 2- and 5-week exposure. Both samples exhibited a decrease in signal amplitude over time, indicating an intrusion of D_2O. However, both $scCO_2$-exposed samples showed a slower intrusion rate as compared to the unreacted cement. After 168 h D_2O

immersion, 4.3 ml and 3.5 ml of water remained in the 2- and 5-week exposed samples, as opposed to 2.3 ml in the untreated sample. This implies an impediment in the flow path due to the alteration in the matrix by scCO$_2$. When comparing both exposed samples, D$_2$O intrusion is the highest after 5 weeks of exposure, with 40 % intrusion versus 27 % after 2 weeks of exposure to scCO$_2$. Finally, comparing the T$_2$ distribution of the untreated and 5 weeks exposed scCO$_2$ cement after 100 % saturation with H$_2$O-brine (Fig. 5) shows that there is a 10 % reduction in pore volume between 0.3 and 10 ms. Assuming carbonate is the main component of the cement and spherical pores (Eq. (3)). Most volume reduction occurs in pore bodies between 3 and 100 nm.

Fig. 6 and Table 2 show the D$_2$O intrusion profile and the derived tortuosity (Eq. (4)). Knowing the effective D$_2$O diffusivity of the untreated cement, the exposed cement effective diffusivity was calculated by using the slope of the intrusion profile (Fig. 6) after 2 days of D$_2$O imbibition. After 2 weeks of exposure, the cement tortuosity increased by a factor of 6, indicating pore blockage. However, the tortuosity increased by only a factor of 3 after 5 weeks compared to the untreated sample, this suggests precipitation of carbonate earlier on and dissolution at a later stage. This observation is consistent with Rimmelé et al. [14] model with an initial sealing stage related to calcium carbonate precipitation plugging the porosity, followed by a dissolution stage marked by a significant increase of porosity.

3.2. Pore structure alteration

MICP (Fig. 7a) and N$_2$ isothermal adsorption (Fig. 7b) measurements on the dried specimens after 5 weeks of exposure confirm that there has been a significant alteration in the flow paths. Fig. 7a shows the reduction in pore throat size peak from 50 nm to 30 nm after 2 weeks indicating a decrease in pore throat size, which suggests that the carbonation process reduces the effective pore volume of the cement. However, after 5 weeks, the average 30 nm pore throat size population has significantly decreased, resulting in the generation of smaller pore throats between 2 and 30 nm. The N$_2$ isothermal adsorption in Fig. 7b shows that the large pores (>30 nm) volume increased after 2 weeks and subsequently decreased after 5 weeks, while only an increase in pore volume is observed in small pores (<30 nm) after 2 and 5 weeks. This implies both dissolution and precipitation in large pores and dissolution only in small pores.

3.3. Chemical and microstructural analysis

Cross-sectional imaging of the cement plug using XCT showed a clear textural distinction between the altered and unaltered cement plug (Fig. 8A-C). After 5 weeks of exposure to scCO$_2$, the plug showed deeper invasion around 10 mm, while after 2 weeks, the invasion depth was only 3 mm. The FTIR analysis (Fig. 9A-C) of the invaded zone revealed the presence of calcite (absorbance peak around 1400 and 875 cm^{-1})

After 5 weeks of exposure, the BSE image presented in Fig. 10 also shows a clear demarcation between the two zones, based on brightness (i.e. proportional to the average atomic number). The invaded zone appears to be darker with a well-defined boundary. The cement matrix (Ca(OH)$_2$ and C–S–H) seems to have been altered after scCO$_2$ exposure. The alteration is visible on the unhydrated grain turning dark in the scCO$_2$-invaded zone. The EDS maps (Fig. 11) performed on the same location confirm that the unhydrated cement grain underwent decalcification and the cement matrix has been enriched in calcium and carbon after scCO$_2$ exposure (see appendix). This finding aligns with the observations made by Kravanja and Knez [35] regarding the disparity in mineral composition, specifically calcium, and carbon, between the CO$_2$-affected and non-affected zones.

Interestingly, magnesium also precipitated (Fig. 11), however, it seems to be located around the carbonated front, suggesting the potential formation of magnesium carbonates. MgO was also present in our cement (Table 1). MgO is often added to cement to improve the mechanical properties and durability of the cement under harsh downhole conditions [36]. Mg(OH)$_2$ can react with scCO$_2$ and form MgCO$_3$ [37]. MgCO$_3$ crystals are insoluble in water and, hence do not easily leach out from the cement [12,38].

4. Discussion

The results show that the interaction between scCO$_2$ and brine-saturated Class G Portland cement leads to significant changes in the
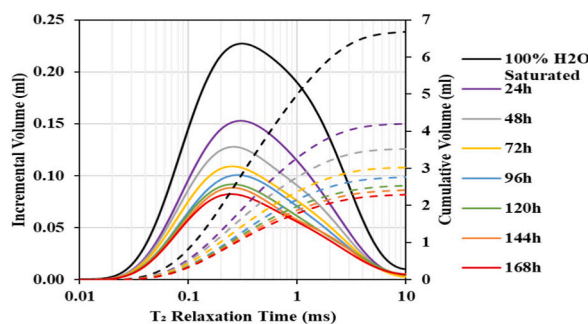

Fig. 3. NMR T$_2$ relaxation distribution of the controlled cement immersed in D$_2$O-brine showing a gradual decrease in volume of the brine as D$_2$O replaces brine inside the cement. Throughout the experiment, the volume of brine decreased from 6.7 to 2.3 ml (dashed curves). a) b).
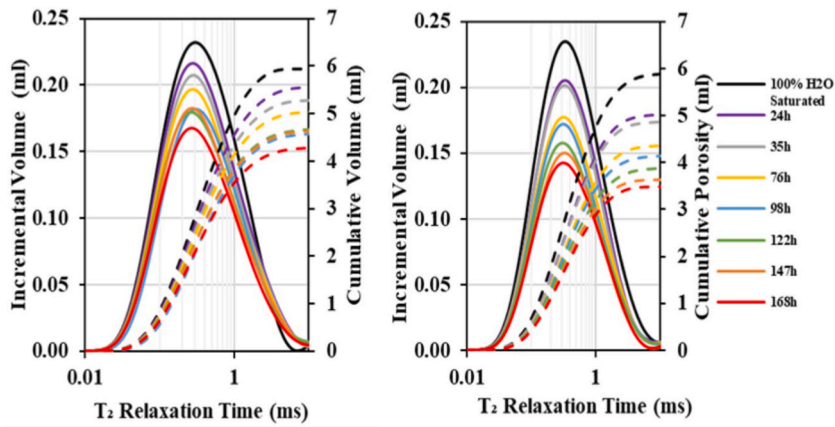
Fig. 4. NMR T_2 relaxation distribution during immersion in D_2O-brine after 2 weeks (a) and 5 weeks (b) exposure to scCO$_2$ showing 40 % vs 27 % D_2O intrusion after 5 weeks and 2 weeks, respectively.
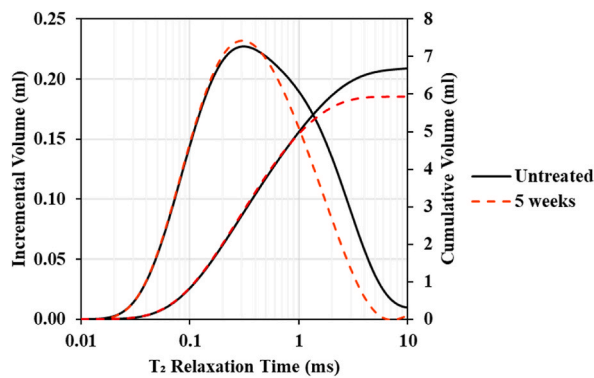

Fig. 5. Comparison between the untreated and 5 weeks scCO$_2$ exposed cement after 100 % saturation with H_2O-brine showed a reduction in a pore volume between 0.3 and 10 ms, resulting in an overall 10 % loss of pore volume after exposure.
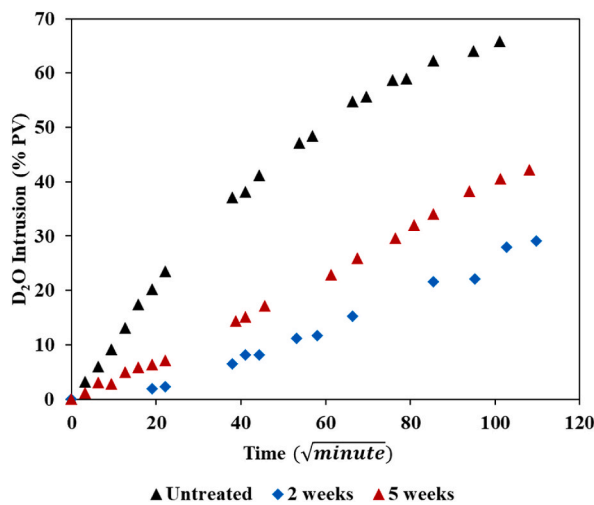

Fig. 6. D_2O intrusion profile on the cement after 2 and 5 weeks-of exposure to scCO$_2$ at 65 °C and 20.7 MPa, showing D_2O flow reduction after scCO$_2$ exposure.

Table 2
Derived tortuosity from Fig. 6. The tortuosity increased by 6 and only by 3 after 2 and 5 weeks, respectively. This suggests an initial precipitation of calcium carbonate and a later dissolution.

Cement	Effective D_2O diffusion (m^2/s)	Tortuosity
Untreated	1.20E-10	4.4
2 weeks	3.09E-12	27.3
5 weeks	1.45E-11	12.6

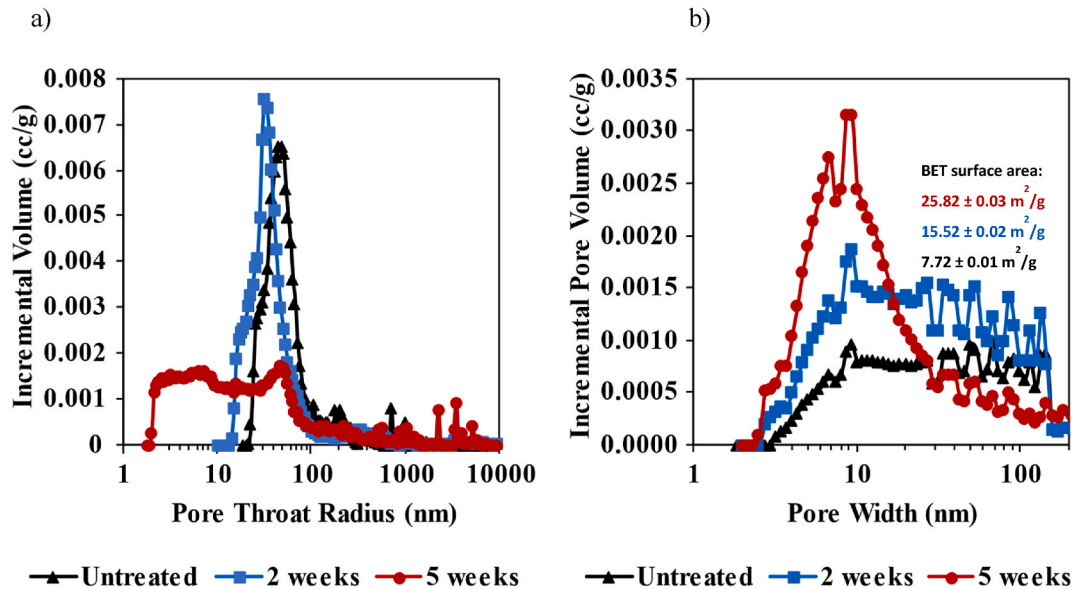a)   b)

Fig. 7. (a) MICP pore throats and (b) DFT pore body size distribution after 2- and 5-weeks exposure to $scCO_2$ at 65 °C and 20.7 MPa. MICP data shows a decrease in pore throat size (ie: connectivity) of the cement after carbonation. N_2 isothermal adsorption shows initial dissolution and later precipitation of $CaCO_3$ in large pores (>30 nm), while only dissolution in small pores (2–30 nm).
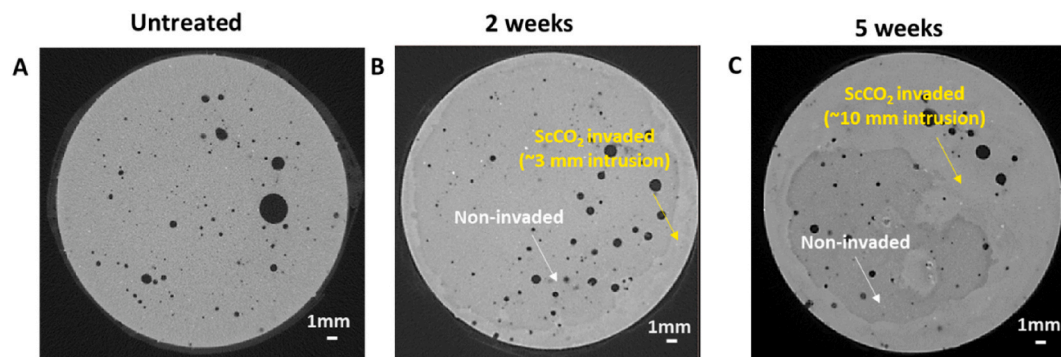

Fig. 8. XCT images of the cement samples showing the $scCO_2$ invaded (yellow arrow) and the non-invaded (white arrow) after 2 weeks (B) and 5 weeks (C) exposure to $scCO_2$ at 65 °C and 20.7 MPa. A deeper invasion is observed after 5 weeks. Note: Each cross section was taken 0.25 inches from the top of the plugs to capture the $scCO_2$ front. (For interpretation of the references to colour in this figure legend, the reader is referred to the Web version of this article.)

pore structure due to mineralization. Analysis of D_2O and tortuosity data indicates that the cement network undergoes calcium carbonate precipitation after 2 weeks, resulting in an increase in cement tortuosity from 4 to 27 ± 2. However, after 5 weeks, the cement tortuosity decreases to 12 ± 2, suggesting a dissolution process. This observation aligns well with the two-stage connectivity evolution proposed by Rimmelé et al. [14], where an initial sealing stage occurs, associated with porosity plugging caused by calcium carbonate precipitation, followed by a reopening of pore entrances during the dissolution phase. The 2-stage porosity could also be pore size dependent, as shown in the BET data. The small pores (2–30 nm) seem to have undergone precipitation and dissolution of $CaCO_3$, while the larger pores (>30 nm) are in the initial phase of precipitation of $CaCO_3$.
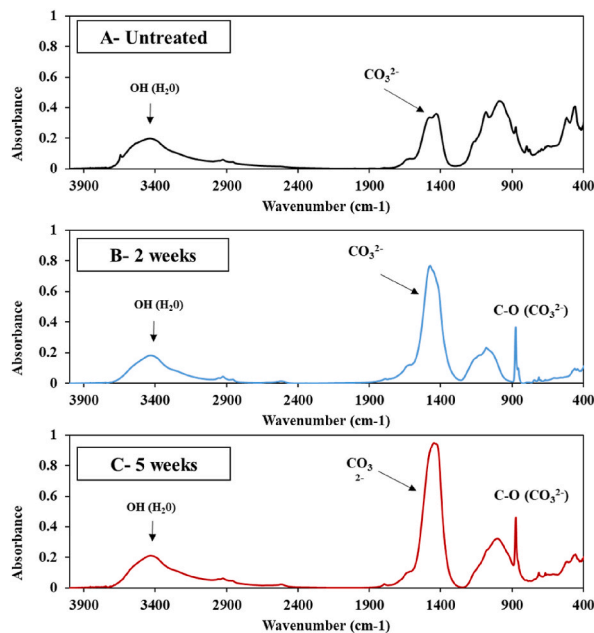
Fig. 9. FTIR mineralogy of the cement (A) untreated, (B) after 2 weeks, and (C) 5 weeks exposure to scCO$_2$, showing calcite absorbance bands around 1400 cm^{-1}, and 875 cm^{-1}.
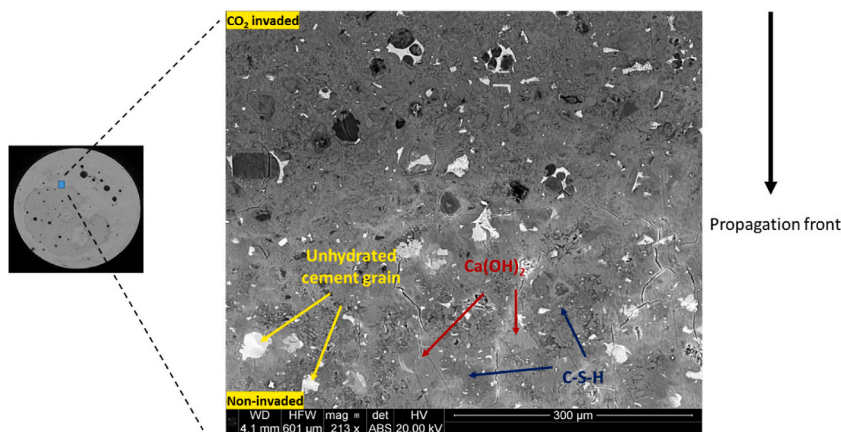

Fig. 10. Backscattered electron image after 5 weeks of exposure to scCO$_2$ at 65 °C and 20.7 MPa. Clear textural demarcation can be observed between the invaded and non-invaded zones. The area invaded by scCO$_2$ appears darker, and the cement grain and matrix appear altered, with less CaOH$_2$ and C–S–H. Note: The cement was imaged without coating.

The D$_2$O diffusivity-based approach also confirms a permeability reduction as shown by the increase in tortuosity by a factor of 6 after 2 weeks and by 3 after 5 weeks of scCO$_2$ exposure (Fig. 6), MICP data also shows a reduction of the main pore throat size (50 nm), which would decrease the connectivity of the cement and decrease the accessible pore volume for scCO$_2$ over time.

The tortuosity results (Table 2) and Eq. (4) can also be utilized to calculate the diffusion coefficient of scCO$_2$ following exposure. In storage conditions the effective scCO$_2$ diffusion coefficient with pure water ranges between 4-8x10^{-9} m^2/s [39,40]. Assuming a value of 6×10^{-9} m^2/s the diffusion coefficient is projected to fall within the range of 8.0×10^{-12} to 3.8×10^{-11} m^2/s after 2 and 5 weeks of exposure. This estimation appears one order of magnitude lower than the diffusion coefficient of CO$_2$ of tight sedimentary rocks documented by Fleury and Brosse [22], which ranges from 5×10^{-11} to 5×10^{-10} m^2/s, confirming limited diffusion over time.

The observation even though limited to one type of cement suggests that considering the risk of CO$_2$ leakage through the cement matrix, its migration could be limited due to the alteration in the flow path, as the result of mineralization [2,3]. estimated a slow diffusive transport of the CO$_2$-saturated brine to 1 mm penetration depth after 20–30 years, with the carbonated zone acting as an efficient barrier to further CO$_2$ penetration. Carey et al. [5] observed limited migration of CO$_2$ from extracted plugs from a 30-year-old CO$_2$ Enhanced Oil Recovery (EOR) project in the SACROC West Texas field.
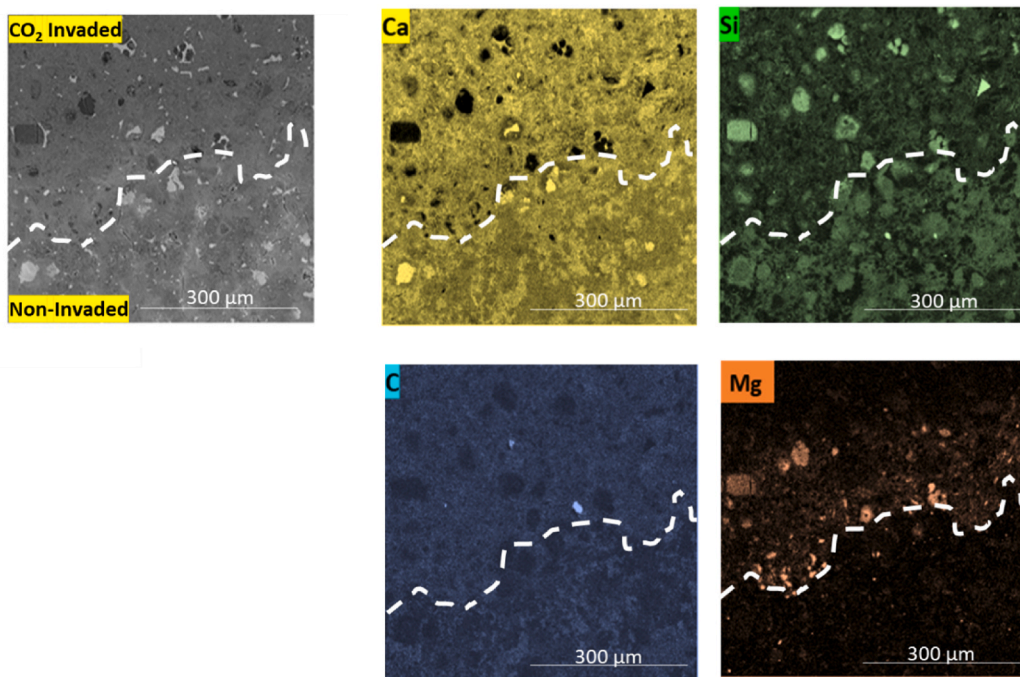
Fig. 11. EDS maps at the boundary between carbonated and non-carbonated zones after 5 weeks of scCO$_2$ exposure at 65 °C and 20.7 MPa. The dashed line represents the scCO$_2$ front. After exposure, the unhydrated cement grains have been decalcified in the scCO$_2$-invaded zone. The invaded zone matrix appears to have less Si but more magnesium and carbon. Note magnesium seems to be localized near the scCO$_2$ front only.

5. Conclusions

In the context of carbon capture and storage, the findings of this study lead to the following conclusions:

- The use of NMR-derived tortuosity proves to be a valuable tool in quantifying the integrity of wellbore cement material for carbon storage.
- Exposure to scCO$_2$ resulted in a decrease in porosity from 37 to 33 %.
- The decrease in average pore throat size confirms a reduction in pore connectivity of the cement.
- The cement tortuosity increased by a factor of 3–6 after 2- and 5 weeks of exposure, confirming pore blockage and slower migration over time.
- The carbonation process was not only time but also pore-size dependent. In smaller pores (<30 nm), only dissolution of calcium carbonate was observed, whereas, in larger pores (30–200 nm), both precipitation and dissolution took place.
- The estimated scCO$_2$ diffusion coefficient in the cement ranged between 8.0×10^{-12} to 3.8×10^{-11} m^2/s after 2 and 5 weeks of exposure.
- After exposure, the invaded zone of the cement matrix appears to be richer in calcium and carbon while only along the invasion front, magnesium concentration seems to increase.

Our proposed methodology for assessing flow path alteration using tortuosity lays the groundwork for future research. Subsequent studies will focus on evaluating changes in mechanical property and dependence of flow path alteration on cement composition under scCO$_2$ conditions.

Data availability

Data associated with the study has not been deposited into a publicly available repository and data will be available upon request.

CRediT authorship contribution statement

Sidi Mamoudou: Writing – review & editing, Writing – original draft, Investigation, Formal analysis. **Mark Curtis:** Writing – review & editing. **Son Dang:** Writing – review & editing. **Chandra Rai:** Writing – review & editing.

Declaration of competing interest

The authors declare that they have no known competing financial interests or personal relationships that could have appeared to influence the work reported in this paper.
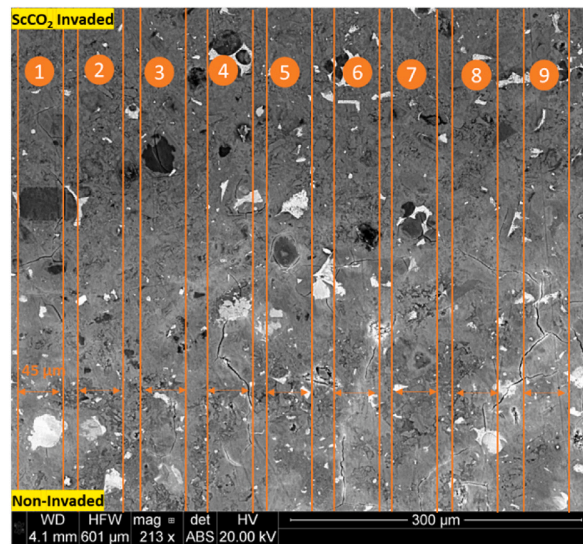
Acknowledgements

Appendix

Fig. A. 9 scan lines were used to determine the elemental profiles (Ca, Si, Mg, and C) over the altered region shown in Figs. 10 and 11. Each line is 45 μm wide (20 pixels) and 500 μm long. Elemental composition was measured by averaging the grayscale intensity of the lines for each component.
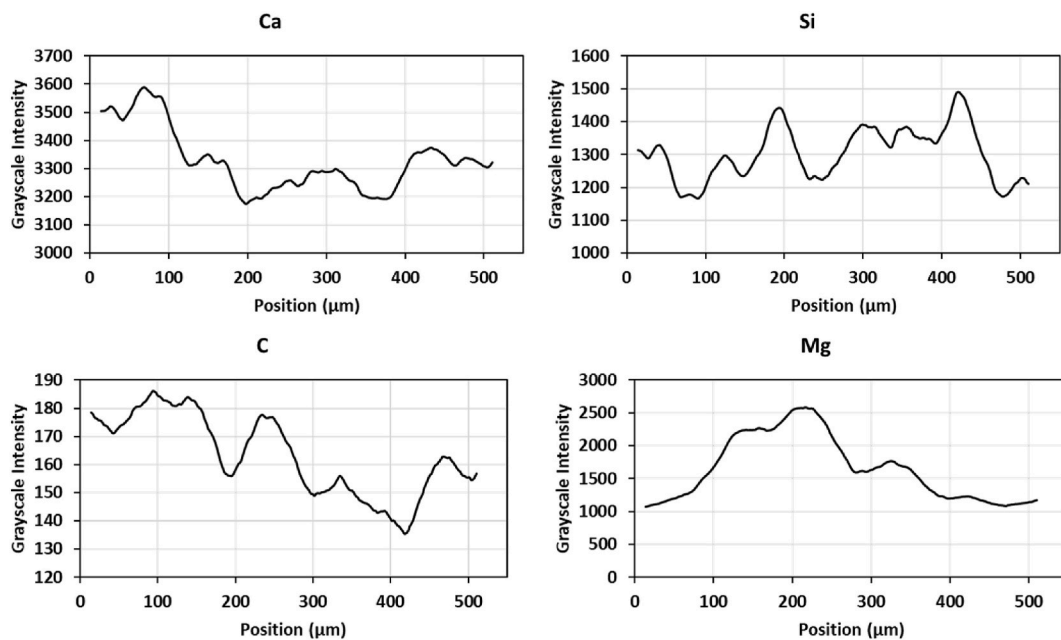
Fig. B. Elemental profiles generated from the X-ray map (Fig.A) of cement exposed to scCO2 at 65 °C and 20.7 MPa for 5 weeks. This data corresponds to an average elemental composition of 9 vertical scans. Position 10 μm corresponds to the top of the SEM image (scCO2-invaded zone), while position 510 μm corresponds to the bottom section of the SEM image (the non-invaded zone) of the cement. The scCO$_2$ invaded zone appears richer in calcium and carbon mostly. Mg is also present near the carbonation front (≈200 μm).

References

[1] T.K. Perkins, O.C. Johnston, A Review of Diffusion and Dispersion in Porous Media, Society of Petroleum Engineers, 1963, p. 480. -PA SPE Journal Paper.

[2] B.G. Kutchko, B.R. Strazisar, D.A. Dzombak, G.V. Lowry, N. Thaulow, Degradation of well cement by CO$_2$ under geologic sequestration conditions, Environ. Sci. Technol. 41 (2007) 4787–4792, https://doi.org/10.1021/es062828c.

[3] B.G. Kutchko, B.R. Strazisar, G.V. Lowry, D.A. Dzombak, N. Thaulow, Rate of CO$_2$ attack on hydrated class H well cement under geologic sequestration conditions, Environ. Sci. Technol. 42 (2008) 6237–6242, https://doi.org/10.1021/es800049r.

[4] B.G. Kutchko, B.R. Strazisar, S.B. Hawthorne, C.L. Lopano, D.J. Miller, J.A. Hakala, G.D. Guthrie, H$_2$S–CO$_2$ reaction with hydrated class H well cement: acid–gas injection and CO$_2$ co-sequestration, Int. J. Greenh. Gas Control 5 (2011) 880–888, https://doi.org/10.1016/j.ijggc.2011.02.008.

[5] W.J. Carey, K. Wigand, S.J. Chipera, G. Woldegabriel, P. Pawar, P.C. Lichtner, S.C. Wehner, M.A. Raines, Jr Guthrie, G D, Analysis and performance of oil well cement with 30 years of CO$_2$ exposure from the Sacroc unit, West Texas, USA, Int. J. Greenh. Gas Control I (1) (2006) 75–85, https://doi.org/10.1016/S1750-5836(06)00004-1, 2007.

[6] A. Duguid, G.W. Scherer, Degradation of oil well cement due to exposure to carbonated brine, Int. J. Greenh. Gas Technol. 4 (2010) 546–560, https://doi.org/10.1016/j.ijggc.2009.11.001.

[7] F. Gherardi, P. Audigane, E.C. Gaucher, Predicting long-term geochemical alteration of wellbore cement in a generic geological CO$_2$ confinement site: tackling a difficult reactive transport modeling challenge, J. Hydrol. 420–421 (2012) (2012) 340–359, https://doi.org/10.1016/j.ijggc.2016.10.018.

[8] S.D.C. Walsh, W.L.D. Frane, H.E. Mason, S.A. Carroll, Permeability of wellbore-cement fractures following degradation by carbonated brine, Rock Mech. Rock Eng. 46 (2013) 455–464, https://doi.org/10.1007/s00603-012-0336-9.

[9] S. Caroll, J.W. Carey, D.A. Dzombak, N.J. Huerta, L. Li, W. Um, S.D.C. Walsh, L. Zhang, Review: role of chemistry, mechanics, and transport on well integrity in CO$_2$ storage environments, Int. J. Greenh. Gas Control 49 (2016) 149–160, https://doi.org/10.1016/j.ijggc.2016.01.010.

[10] W. Um, A. Rod Rod, H.B. Jung, C.F. Brown, Geochemical alteration of wellbore cement by CO$_2$ or CO$_2$ + H$_2$S reaction during long-term carbon storage, Greenhouse Gas Sci Technol 6 (2016) 1–14, https://doi.org/10.1002/ghg.1595.

[11] A. Duguid, W. Zaluski, G. El-Kaseeh, S.Y. Lee, M. Piercy, Well integrity risk assessment to inform containment risk monitoring for carbon capture, utilization, and storage, applied to the Weyburn-Midale Field, Canada, Int. J. Greenh. Gas Technol 86 (2019) (2019) 226–238, https://doi.org/10.1016/j.ijggc.2016.10.018.

[12] R. Ahmed, S. Shah, S. Osisanya, S. Hassani, O. Omosebi, R. Elgaddafi, H. Maheshwari, A. Srivastava, J. Hwang, M. Sharma, Effect of H$_2$S and CO$_2$ in HPHT wells on tubulars and cement, Final project report, prepared under US Department of Interior Bureau of Safety and Environmental Enforcement project (2015). E12PC00035.

[13] V. Barlet-Gouédard, G. Rimmelé, B. Goffé, O. Porcherie, Mitigation Strategies for Risk of CO$_2$ Migration through Wellbores, Presented at IADC/SPE Drilling Conference, Miami, Florida, USA, 2006, https://doi.org/10.2118/98924-MS. SPE-98924-MS.

[14] G. Rimmelé, V. Barlet-Gouédard, O. Porcherie, B. Goffé, F. Brunet, Heterogeneous porosity distribution in Portland cement exposed to CO$_2$-rich fluids, Cem. Concr. Res. 38 (2008) 1038–1048.

[15] M. Wigand, J.P. Kaszuba, J.W. Carey, W.K. Hollis, Geochemical effects of CO$_2$ sequestration on fractured wellbore cement at the cement/caprock interface, Chem. Geol. 265 (2009) 122–133.

[16] N.J. Huerta, M.A. Hesse, S.L. Bryant, B.R. Strazisar, C.L. Lopano, Experimental evidence for self-limiting reactive flow through a fractured cement core: implications for time-dependent wellbore leakage, Environ. Sci.Technol. 47 (2013) 269–275, https://doi.org/10.1021/es3013003.

[17] L. Luquot, H. Abdoulghafour, P. Gouze, Hydro-dynamically controlled alteration of fractured Portland cements flowed by CO$_2$-rich brine, Int. J. Greenh. Gas Control 16 (2013) 167–179, https://doi.org/10.1016/j.ijggc.2013.04.002.

[18] H.E. Mason, W.L. Du Frane, S.D.C. Walsh, Z. Dai, S. Charnvanichborikarn, S.A. Carroll, Chemical and mechanical properties of wellbore cement altered byCO$_2$-rich brine using a multianalytical approach, Environ. Sci. Technol. 47 (2013) 1745–1752, https://doi.org/10.1021/es3039906.

[19] S.D.C. Walsh, H.E. Mason, W.L. Du Frane, S.A. Carroll, Experimental calibration of a numerical model describing the alteration of cement/caprock interfaces by carbonated brine, Int. J. Greenh. Gas Control 22 (2014) 176–188, https://doi.org/10.1016/j.ijggc.2014.01.004.

[20] S.D.C. Walsh, H.E. Mason, W.L. Du Frane, S.A. Carroll, Mechanical and hydraulic coupling in cement–caprock interfaces exposed to carbonated brine, Int. J. Greenh. Gas Control 25 (2014) 109–120, https://doi.org/10.1016/j.ijggc.2014.04.001.

[21] C. Gallé, Effect of drying on cement-based pore structure as identified by mercury intrusion porosimetry A comparative study between oven-, vacuum-, and freeze-drying, Cement Concr. Res. 31 (2001) 1467–1477.

[22] M. Fleury, E. Brosse, Transport in tight rocks. Geophysical Monograph Series, AGU Advancing Earth and Space Sciences, 2017, https://doi.org/10.1002/9781119118657.ch2.

[23] A. Ichim, K.F. Saleh, C. Teodoriu, C. Sondergeld, The need of NMR cement properties characterization and lesson learned. *Proc.,* SPE Oklahoma City Oil and Gas Symposium, 2019, https://doi.org/10.2118/195228-MS.

[24] N.C. Collier, J.H. Sharp, N.B. Milestone, J. Hill, I.H. Godfrey, The influence of water removal techniques on the composition and microstructure of hardened cement pastes, Cement Concr. Res. 38 (6) (2008) 737–744.

[25] R. Blinc, M. Burgar, G. Lahajnar, N. Rozmarin, V. Rutar, I. Kocuvan, J. Ursic, NMR relaxation study of adsorbed water in cement and C3S pastes, J. Am. Ceram. Soc. 61 (1–2) (1978) 35–37. https://ceramics.onlinelibrary.wiley.com/doi/abs/10.1111/j.1151-2916.1978.tb09224.x.

[26] K.J. Dunn, D.J. Bergmann, G.A. Latorraca, Nuclear Magnetic Resonance: Petrophysical and Logging Applications, Handbook of Geophysical Exploration, vol. 32, Pergamon, New York, 2002, p. 293.

[27] D. Chang, H. Vinegar, Effective porosity, producible fluid and permeability in carbonates from NMR logging, SPWLA 35th annual logging symposium, June 19–22 (1994) pp21.

[28] A. Matteson, J.P. Tomanic, M. Herron, D.F. Allen, W.E. Kenyon, NMR Relaxation of Clay-Brine Mixtures, SPE49008, 1998, pp. pp205–211.

[29] R. Kleinberg, Utility of NMR T$_2$ distributions, connection with capillary pressure, clay effect, and determination of the surface relaxivity parameter ρ2, Magn. Reson. Imag. 14 (1996) 761–767.

[30] S. Dang, S. Mukherjee, C.H. Sondergeld, C.S. Rai, Measurement of effective tortuosity in unconventional tight rock using nuclear magnetic resonance. Presented at the Unconventional Resources Technology Conference (URTeC), July, Houston, Texas, USA, 2021, pp. 26–28, https://doi.org/10.15530/urtec-2021-5118. URTEC-2021-5118-MS.

[31] J. Odiachi, Tortuosity of Tight Rocks. MS Dissertation, The University of Oklahoma, Norman, Oklahoma, 2022.

[32] M.E. Baur, C.W. Garland, W.H. Stockmayer, Diffusion coefficients of H$_2$O-D$_2$O mixtures, J. Am. Chem. Soc. 81 (12) (1959) 3147–3148, https://doi.org/10.1021/ja01521a058.

[33] C.H. Sondergeld, C.S. Rai, A new concept of quantitative core characterization, Lead. Edge 12 (7) (1993) 774–779.

[34] A. Sinha, Surface area study in organic-rich shales using nitrogen adsorption. MS Thesis, The University of Oklahoma, Norman, Oklahoma, 2017.

[35] G. Kravanja, Z. Knez, Carbonization of class G well cement containing metakaolin under supercritical and saturated environment, Construct. Build. Mater. 376 (2023), https://doi.org/10.1016/j.conbuildmat.2023.131050.

[36] A. Buntoro, R.S. Rubiandini, The effect of neat magnesium oxide (MgO) as expanding additive on cement shear bond strength at high temperature up to 2500C, World Geothermal Congress. Kyushu, Tohoku, Japan, May 28-June 10 (2000).

[37] M.G. Gardeh, A.A. Kistanov, H. Nguyen, H. Manzano, W. Cao, P. Kinnunen, Exploring mechanism of hydration and carbonation of MgO and $Mg(OH)_2$ in reactive magnesium oxide-based cements, The Journal of Physical Chemistry C 2022 126 (14) (2022) 6196–6206, https://doi.org/10.1021/acs.jpcc.1c10590.

[38] P.N. Cheremisinoff, Handbook of Water and Wastewater Treatment Technology, Marcel Decker Inc, New York, 1995.

[39] Shane P. Cadogan, Geoffrey C. Maitland, J.P. Trusler, Martin, Diffusion coefficients of CO2 and N2 in water at temperatures between 298.15 K and 423.15 K at pressures up to 45 MPa, J. Chem. Eng. Data 59 (2) (2014) 519–525.

[40] S. Zharghami, F. Boukadi, Y. Al- Wahaibi, Diffusion of carbon dioxide in formation water as a result of CO_2 enhanced oil recovery and CO_2 sequestration, J. Pet. Explor. Prod. Technol. 7 (2016) 161–168, https://doi.org/10.1007/s13202-016-0261-7.